Structural details and magnetic order of $La_{1-x}Sr_xCoO_3$ ($x \leqslant 0.3$)

R. Caciuffo, D. Rinaldi, and G. Barucca
Istituto Nazionale per la Fisica della Materia and Dipartimento di Scienze dei Materiali e della Terra, Università di Ancona, Via Brecce Bianche I-60131, Ancona, Italy

J. Mira and J. Rivas
Departamento de Física Aplicada, Universidade de Santiago, E-15706 Santiago de Compostela, Spain

M. A. Señarís-Rodríguez
Departamento Quimica Fundamental e Industrial, Universidade da Coruña, E-15071 A Coruña, Spain

P. G. Radaelli
ISIS Facility, Rutherford Appleton Laboratory, OX11 0QX Chilton, United Kingdom

D. Fiorani
Istituto di Chimica dei Materiali, Consiglio Nazionale delle Ricerche, P.O.B. 10, I-00016 Monterotondo Stazione, Roma, Italy

J. B. Goodenough
Center for Materials Science and Engineering, University of Texas at Austin, Austin, Texas 78712-1063
(Received 17 June 1998; revised manuscript received 1 September 1998)

The crystallographic structure and the magnetic order of the distorted perovskite $La_{1-x}Sr_xCoO_3$ ($0.10 \leqslant x \leqslant 0.30$) has been studied by neutron diffraction, high-resolution electron microscopy, and magnetic-susceptibility measurements. The results give direct evidence for an inhomogeneous distribution of the Sr^{2+} ions and the segregation of the material into hole-rich ferromagnetic regions and a hole-poor semiconducting matrix at lower values of x. The holes introduced by Sr doping are attracted to the Sr^{2+} ions where they stabilize to lowest temperatures an intermediate-spin state at neighboring trivalent cobalt. The antibonding e electrons so stabilized increase the mean unit-cell volume and are delocalized over the cobalt atoms of the cluster where they couple the localized t^5 configurations ferromagnetically. Long-range ferromagnetic order between clusters is realized even for Sr doping as low as $x=0.10$. The transition to a spin glass state is observed only for Sr concentrations smaller than 0.10. The volume of a hole-rich cluster grows in a magnetic field, and the origin of the large negative magnetoresistance observed near T_C for $0.15 \leqslant x \leqslant 0.25$ appears to be due to a growth of the clusters to a percolation threshold. For $x=0.30$, the σ^* band of the intermediate-spin state below T_C is at the threshold of a transition from itinerant to polaronic conduction and, above T_C, the system transforms smoothly to a cluster state. [S0163-1829(99)01002-4]

I. INTRODUCTION

The remarkable electrical transport properties of the mixed-valent pseudocubic perovskites $Ln_{1-x}A_xMnO_3$, Ln=rare earth and A=alkaline earth, have been reported by many groups, for example Refs. 1–6, and have been interpreted[7] in terms of a transition from localized to itinerant e-electron behavior in the presence of localized t^3 configurations ($S=3/2$) at the high-spin Mn-atom configurations of mean t^3e^{1-x} character. In particular, a huge magnetoresistance, so large as to deserve the description ''colossal magnetoresistance'' (CMR), has been observed above a ferromagnetic Curie temperature T_C in mixed-valent compositions having an O-orthorhombic ($c/a>\sqrt{2}$) structure. For a fixed Mn(IV)/Mn ratio, e.g., 0.3, the $AMnO_3$ perovskite evolves across the O-orthorhombic phase from an O′-orthorhombic ($c/a<\sqrt{2}$) phase to an R-rhombohedral phase in a narrow range of increasing mean ionic radius of the A-site cations. In the O′ phase, localized e electrons at Mn^{3+} ions are ordered by cooperative local Jahn-Teller deformations into orbitals oriented in the (001) planes; in the R phase the e electrons occupy a narrow σ^* band of e-orbital parentage. In the O phase, the CMR has its maximum value near the O′-O phase boundary where T_C increases dramatically with increasing mean ionic radius of the A-site cations, the magnetic transition is first order, and the e-electron conductivity changes from polaronic above T_C to that of a bad metal below T_C.

Both theory and experiment have indicated that a first-order transition occurs at the crossover from localized to itinerant electronic behavior. Where the critical temperature for segregation of a localized-electron and an itinerant-electron phase is too low for atomic diffusion, phase segregation may be accomplished by atomic displacements. In transition-metal AMO_3 oxides with the perovskite structure, an oxygen displacement within a (180°-ϕ) M-O-M bond introduces a shorter M-O bond on one side and a longer one on the other. Cooperative oxygen displacements can segregate domains with shorter metal-oxygen bonds from those with longer bonds; and in a mixed-valent system, higher oxidation states

 ©1999 The American Physical Society

are stabilized in the domains with shorter M-O bonds. In this way, an electronic phase segregation is accomplished without the introduction of the chemical inhomogeneities that characterize a conventional phase segregation by atomic diffusion. Moreover, such a phase segregation would allow the phase boundaries to be mobile. Where one phase is ferromagnetic with a Curie temperature significantly higher than the other phase, superparamagnetic clusters may be stabilized above the long-range ordering temperature T_C of the matrix and spin-glass behavior may be found below T_C in the absence of any measurable chemical inhomogeneity. Moreover, if the superparamagnetic clusters are rich in itinerant charge carriers and the short-range cooperative atomic displacements are dynamic, the application of a magnetic field may enlarge the volume of the superparamagnetic clusters to beyond their percolation threshold to give a CMR. Such a situation has been suggested[7] to be responsible for the CMR phenomenon in the manganese-oxide perovskites. The present work was undertaken to see whether such an interpretation would be applicable in another perovskite system exhibiting a CMR.

A large magnetoresistance observed in $La_{1-x}Sr_xCoO_3$ thin films at doping $0.15<x\leqslant 0.20$ (Ref. 8) has stimulated a reinvestigation of this perovskite system.[9–15] A reexamination of the $La_{1-x}Sr_xCoO_3$ phase diagram was also made[16,17] just prior to the report of a large magnetoresistance. $LaCoO_3$ had been known to exhibit remarkable transport and magnetic properties as a result of thermally induced transitions from a low-spin (LS) to a high-spin (HS) or intermediate-spin (IS) state at the trivalent cobalt atoms.[18] Sr doping stabilizes the IS spin state.[19]

At room temperature and below, the parent compound $LaCoO_3$ is an insulator with a rhombohedral ($R\bar{3}c$) perovskite structure.[20] At lowest temperatures the trivalent cobalt are all in the LS $^1A_1$ state ($t_2^6\sigma^{*0}$; $S=0$) with no long-range magnetic order.[21,22] With a uniform LS distribution, the empty e orbital can be anticipated to form a narrow antibonding σ^* band of itinerant electron states that are strongly hybridized with the O $2p_\sigma$ orbitals. A small energy separation between the LS state and the HS $^5T_2$ state ($t_2^4e^2$;$S=2$) allows thermal excitation of HS configurations that increase in population with temperature.[18] It was postulated early[23] that the displacement of oxygen atoms away from the HS configurations with localized e^2 (or e^1 at an IS ion) would stabilize LS configurations at neighboring cobalt atoms, but no static ordering of LS and HS (or IS) ions has been observed. On the other hand, Mössbauer data[24] distinguished two kinds of trivalent cobalt atoms below 100 K, and infrared spectroscopy[25] has identified dynamic Jahn-Teller deformations at localized IS ($t_2^5e^1$) configurations rather than dynamic breathing modes of HS ($t_2^4e^2$) configurations. Moreover, the bulk conductivity and dielectric properties below 350 K support polaronic charge transport.[26] In the temperature range $350<T<650$ K, the transport properties of $LaCoO_3$ change smoothly from that of a thermally activated semiconductor to that of a metal, a metallic temperature dependence becoming stable above 650 K.[18] This change may be attributed[17,18] to a transition, as the polaron population exceeds 50%, from localized IS configurations coexisting with LS configurations at nearest neighbors to a uniform IS state ($t_2^5\sigma^{*1}$; $S=1$). If the Fermi energy of the σ^* band intersects the t^5 energy level in this model, the system would correspond to an ''intermediate-valence'' state (to use rare-earth terminology) $t_2^{5-\delta}\sigma^{*1+\delta}$ having a mean spin $S=1+\delta$ with a δ that increases with temperature. The parameter δ would correspond to the fraction of HS state admixed with the IS state.

Substitution of Sr^{2+} for La^{3+} in $La_{1-x}Sr_xCoO_3$ oxidizes the CoO_3 array. The evolution with Sr doping of the magnetic and transport data has been interpreted as follows.[16] (i) For $0<x<0.1$, the holes introduced into the CoO_3 array stabilize to lowest-temperature IS clusters that are trapped at Sr^{2+} ions; the IS clusters become superparamagnetic below a ferromagnetic Curie temperature $T_C\approx 230$ K, which indicates the clusters are isolated from one another. (ii) In the range $0.1\leqslant x\leqslant 0.18$, the IS clusters become larger, each containing several holes, and interactions between isolated superparamagnetic clusters give a spin-glass behavior below a temperature $T_g<T_C$. A collective freezing of the cluster moments below T_g via frustrated intercluster interactions has been confirmed,[27] but whether the large IS clusters are Sr^{2+}-rich has not been established. (iii) In the range $0.18<x\leqslant 0.25$, the size of the IS clusters appears to vary with temperature below T_C so as to pass through a temperature range where, in zero applied field, the volume of the metallic clusters exceeds the percolation threshold. In this compositional range, the ferromagnetic clusters are coupled ferromagnetically to one another below a metal-insulator transition at $T_{MI}<T_C\approx 240$ K, where T_{MI} increases to T_C with increasing x. (iv) For $x>0.25$, the percolation threshold for the ferromagnetic metallic clusters is exceeded at all temperatures $T<T_C$, as has also been confirmed.[27] A powder neutron-diffraction study has also confirmed the presence of long-range ferromagnetic order for $x>0.2$, but no magnetic scattering was observed at lower doping levels.[28]

As in conventional metallic ferromagnets, samples with $x>0.25$ have a resistivity versus temperature curve that changes slope at T_C where spin-disorder scattering saturates.[14] Samples with dopings $0.2<x<0.4$ show a small, negative magnetoresistance ($|\Delta\rho/\rho|<10\%$ in a magnetic field of 6 T) that becomes positive at $x\approx 0.5$.[15] Larger values of the magnetoresistance (up to $|\Delta\rho/\rho|\approx 40\%$ for $B=6$ T) were observed as the doping approaches $x=0.2$, the composition where the ferromagnetic IS clusters approaches their percolation threshold in zero applied field.[29] Correlation of the large magnetoresistance with a loss of metallic conductivity was attributed to the loss of long-range ferromagnetic order for $x<0.2$,[15,29] which is consistent with a loss of percolation in zero field of the metallic IS clusters.

To determine the details of the structural changes induced by doping with Sr the $LaCoO_3$ parent compound and to check whether magnetic ordering of any kind could be detected for doping levels $x<0.2$, we have performed a neutron-diffraction experiment on samples of $La_{1-x}Sr_xCoO_3$ ($x=0.10$, 0.15, 0.20, 0.25, and 0.30) under better conditions for instrumental resolution and sensitivity than those reported in Ref. 28. The neutron experiments have been complemented by high-resolution transmission electron microscopy and by measurements of the linear and nonlinear components of the complex magnetic susceptibility. The re-

sults have allowed a complete crystallographic study and revealed that ferromagnetic order is indeed present at low temperature even in the $x=0.10$ sample, although with a strongly reduced ordered moment. Information on the spin state of the trivalent Co ions has been obtained from the variation with x of the Co-O distance and the volume of the unit cell. A peculiar behavior has been observed for the $x=0.30$ sample for temperatures higher than the Curie point $T_C=227$ K, where the lattice thermal expansion deviates from the Grüneisen behavior and the equilibrium Co-O bond length dramatically increases. These observations, together with large departures of the magnetic susceptibility from the Curie-Weiss law and the sudden growth of a temperature-dependent component in the small-angle neutron scattering distribution, are taken as evidence for the formation of isolated magnetic clusters and a transition from itinerant-electron to polaronic conduction at T_C.

II. EXPERIMENTAL PROCEDURE

The specimens of $La_{1-x}Sr_xCoO_3$ ($x=0.10$, 0.15, 0.20, 0.25, and 0.30) used in the present study were prepared by a coprecipitation method from La_2O_3, $Co(NO_3)_26H_2O$, and $SrCO_3$ as starting materials, following the procedure described in Ref. 16. (See *Note added in proof.*) A small amount of a sample with $x=0.05$ was also prepared by the same method for magnetic susceptibility measurements. The products were fully characterized by x-ray-diffraction, differential thermal analysis, thermogravimetry, iodometric titration under nitrogen atmosphere, electron microscopy, and ac magnetic susceptibility measurements. The samples were stoichiometric and thermally stable; no evidence for any impurity phase was found in either x-ray or neutron diffraction. Particle size and morphology were studied with a JEOL 6400 scanning electron microscope, which revealed individual particles with quite perfect spherical shape and size between 700 and 900 nm.

The linear and nonlinear components of the ac magnetic susceptibility were measured as a function of temperature with a Lake Shore 7000 system using the mutual-inductance technique. Data were collected on warming from 13 to 300 K after zero-field cooling of the sample. The calibration was performed with a $Gd_2(SO_4)_38H_2O$ paramagnetic standard having the same shape and size as the investigated samples.

High-resolution transmission electron microscopy observations were carried out on the $x=0.30$ and 0.15 samples at room temperature with a Philips CM200 microscope offering a point-to-point resolution of 0.27 nm.

The neutron powder-diffraction experiments were carried out on the high-resolution neutron diffractometer D2B and the medium-resolution, high-intensity diffractometer D20 of the Institute Laue-Langevin (ILL), in Grenoble, France, covering the angular range $5°<2\theta<165°$ with incident neutrons of wavelength $\lambda=1.5943(1)$ Å and $\lambda=2.4062(5)$ Å, respectively. On both instruments, data were collected at several temperatures on warming from 2.5 to 300 K with the sample contained in a 5-mm-diam, cylindrical vanadium can inside a helium cryostat.

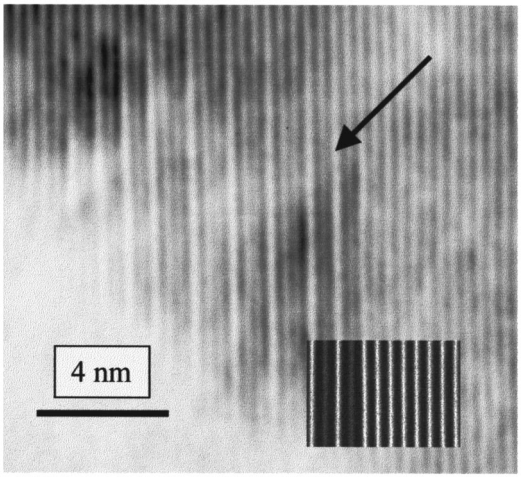

FIG. 1. HREM image taken along the [0 −1 1] zone axis for $La_{0.7}Sr_{0.3}CoO_3$. The periodicity of the bright fringes changes with the spatial position inside the sample, indicating an inhomogeneous distribution of the La ions. The observation can be simulated assuming the presence of aperiodically alternate Sr-rich and La-rich (0 1 1) planes, as shown in the inset.

III. ELECTRON MICROSCOPY

High-resolution electron microscopy (HREM) was used to analyze samples with Sr content $x=0.15$ and 0.30 in a search for possible segregation or ordering between the La^{3+} and Sr^{2+} cations. No superstructure spots were detected in any of the various crystallites selected and oriented along different zone axes. However, evidence for the presence of hole-rich regions imbedded in a hole-poor matrix was obtained from the observation of bright fringes with nonuniform periodicity in HREM micrographs taken along the $[0-1\ 1]$ zone axis (Miller indices referred to the rhombohedral cell). One of the images recorded for the $x=0.30$ sample is shown in Fig. 1. The different spacing between the bright fringes in the matrix and in the region indicated by the arrow cannot be accounted for either by variations in the sample thickness or by crystallographic defects. On the other hand, the observations can be locally simulated by assuming the presence of aperiodically alternate Sr-rich and La-rich (0 1 1) planes. Different periodicity for the bright fringes can be obtained by changing the repetition ratio between Sr-rich and La-rich planes. Simulations of this kind have been performed with the EMS software package,[30] and an example of the results obtained is shown in the inset of Fig. 1. Hole-rich regions with sizes ranging from 8 to 40 nm were detected in both the $x=0.15$ and the $x=0.30$ samples.

IV. MAGNETIC SUSCEPTIBILITY

On the basis of magnetization measurements, the magnetic phase diagram of $La_{1-x}Sr_xCoO_3$ has been divided into a spin-glass region for $0\leqslant x<0.10$ and a cluster-glass region for $0.10\leqslant x\leqslant 0.6$,[31,32] the appearance of the spin-glass state being ascribed to the frustration of random exchange interactions.

Our susceptibility measurements indicate that a spin-glass behavior can be assumed only at very low Sr doping, a more complex phenomenology emerging already at $x=0.10$. The

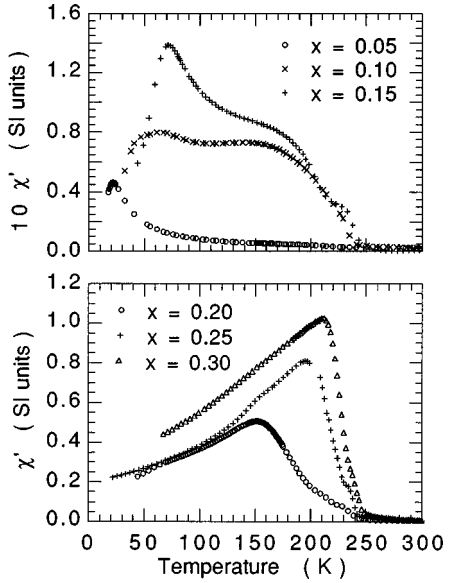

FIG. 2. Real part of the linear magnetic ac susceptibility as a function of temperature for $La_{1-x}Sr_xCoO_3$ ($0.05 \leqslant x \leqslant 0.30$). Data were taken with a driving field of amplitude $H_0 = 3.75$ Oe oscillating at a frequency of 1 kHz.

real part of the linear magnetic ac susceptibility, χ', and the magnitude of the third-harmonic nonlinear susceptibility, $|(\frac{3}{4})\chi_3 H_0^2|$, are shown as functions of temperature in Fig. 2 and Fig. 3 for samples with $0.05 \leqslant x \leqslant 0.30$. The linear component was measured with a driving field of amplitude $H_0 = 3.75$ Oe oscillating at a frequency of 1 kHz. The nonlinear term was obtained from the third harmonic of the voltage induced in the pickup coils by the time-varying sample magnetization. The primary coil was driven at a fundamental frequency $f = 9$ kHz while the reference input to the lock-in amplifier, set to a band-pass filter mode of operation, was at a frequency $3f$.

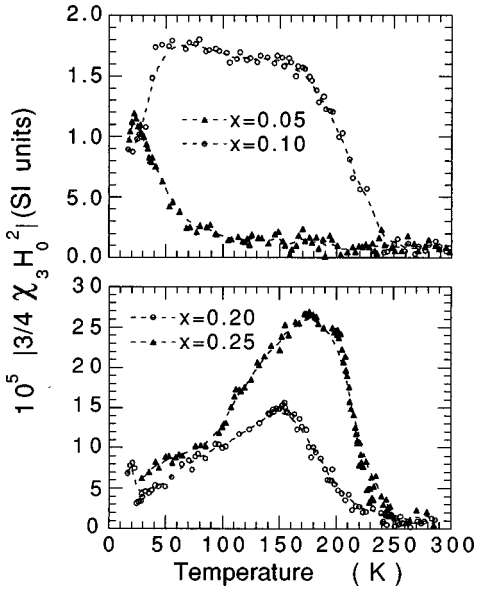

FIG. 3. Magnitude of the third-harmonic nonlinear susceptibility measured for $La_{1-x}Sr_xCoO_3$ ($0.05 \leqslant x \leqslant 0.30$) as a function of temperature. Data were taken with a driving field of amplitude $H_0 = 1.25$ Oe oscillating at a frequency of 9 kHz.

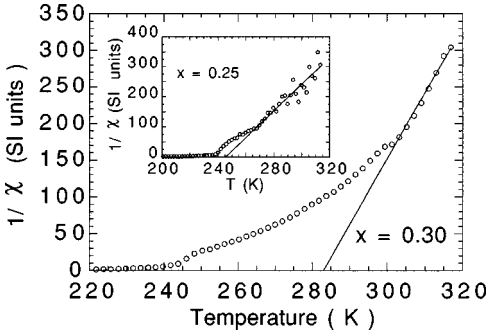

FIG. 4. Temperature dependence of the inverse magnetic susceptibility $1/\chi$ for $La_{0.7}Sr_{0.3}CoO_3$ and $La_{0.75}Sr_{0.25}CoO_3$ (inset). The solid line is a fit to the Curie-Weiss law. Deviations from the linear behavior above T_C are due to strong fluctuations in the magnetic order parameter.

For $x = 0.05$, the linear susceptibility has a shape that is usually observed in spin-glass systems, with a sharp cusp at a temperature $T_g \approx 20$ K. The hypothesis of a spin-glass state at this composition is supported by the behavior of the nonlinear susceptibility, which also shows a cusp around 20 K. As the freezing temperature T_f is approached, the mean-field theory for spin glasses anticipates a critical divergence for $|\chi_3|$ according to the power law $[(T-T_f)/T_f]^{-\gamma}$. In the present case, we obtain a critical exponent $\gamma = 1.1$, which compares favorably with the values obtained for canonical spin-glass systems.[33] A freezing of the magnetic moments into a spin-glass state has been suggested also for $La_{0.92}Sr_{0.08}CoO_3$, where a polarized neutron scattering study has shown that the paramagnetic scattering increases steadily with decreasing temperature but saturates below 24 K.[22]

The magnetic behavior for $x \geqslant 0.10$ is more complicated. The nonlinear susceptibility component has a rounded shape similar to that observed for $La_{0.5}Sr_{0.5}CoO_3$;[34] it has been attributed to the freezing of ferromagnetic clusters.[32] The onset of the linear susceptibility at about 230 K, steeper and steeper with increasing x, announces ferromagnetic ordering for all the samples. However, the variation with x of the χ' magnitude indicates that the ordered phase occupies only a fraction of the volume; this fraction increases with the Sr content. The maximum near 60 K, observed for $x = 0.10$ and 0.15, indicates spin-glass behavior persisting in the volume of material that is not ferromagnetic. These features become

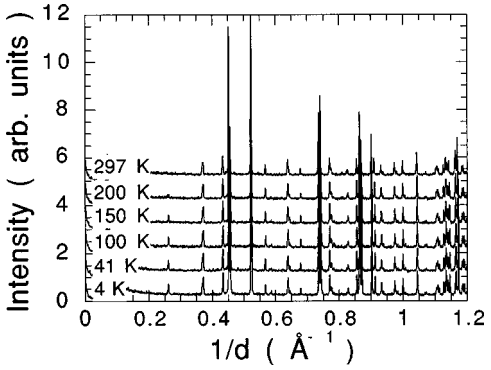

FIG. 5. High-resolution neutron-diffraction patterns recorded at different temperatures for $La_{0.7}Sr_{0.3}CoO_3$; the intensity distribution is plotted as a function of the inverse interplanar spacing $1/d$.

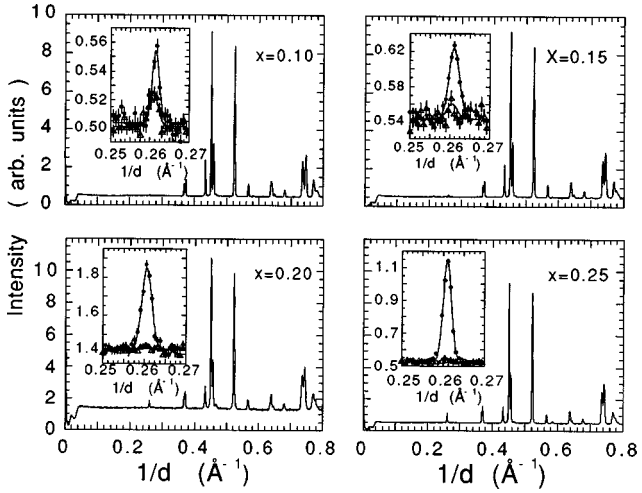

FIG. 6. Neutron-diffraction patterns observed for $La_{1-x}Sr_xCoO_3$ ($x=0.10$, 0.15, 0.20, and 0.25) at $T=15$ K. The (1 1 0) Bragg peak is shown in the inset at 270 K (triangles) and 2 K (dots). The increased intensity at low temperature is due to the ferromagnetic order of the Co magnetic moments.

less and less evident as, with increasing x, the cluster size grows and a percolating network of clusters is formed.

In the samples with $x=0.25$ and 0.30, deviations from the Curie-Weiss law are apparent well above T_C, as is shown in Fig. 4, where the inverse susceptibility is plotted as a function of T. These deviations are similar to those observed for $La_{1-x}Ca_xMnO_3$ (Ref. 35) and suggest the presence of fluctuating short-range-ordered regions.

V. NEUTRON DIFFRACTION

A. Diffraction patterns and data analysis

Selected diffraction patterns recorded on D2B for the $x=0.30$ specimen at different temperatures are shown in Fig. 5. The results obtained at $T=15$ K with D20 for the other investigated $La_{1-x}Sr_xCoO_3$ samples ($x=0.10$, 0.15, 0.20, and 0.25) are shown in Fig. 6. All the observed Bragg peaks can be indexed in the rhombohedral $R\bar{3}c$ space group, with only one Co site. At no temperature or composition was the (1 1 1) reflection (allowed in the $R\bar{3}$ symmetry) observed.

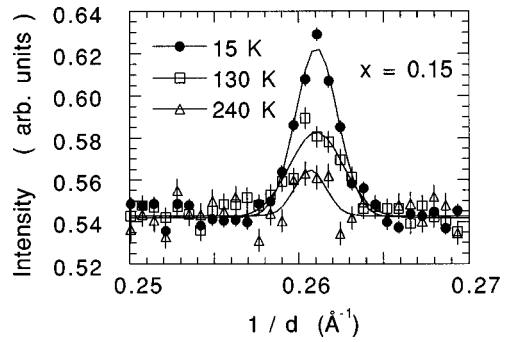

FIG. 7. The (1 1 0) Bragg peak for $La_{0.85}Sr_{0.15}CoO_3$ at three temperatures. The peak is resolution limited above T_C (230 K) and at the lowest temperature. A broadening can be appreciated in the temperature interval between 80 and 230 K.

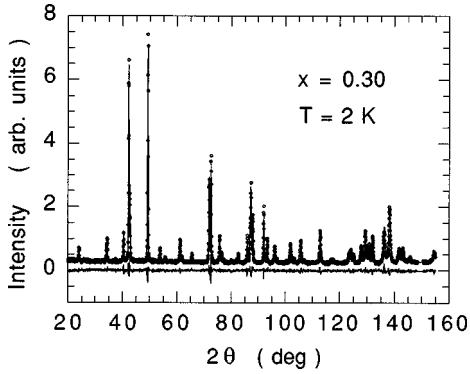

FIG. 8. Observed and calculated neutron-diffraction patterns for $La_{0.7}Sr_{0.3}CoO_3$ at 2 K. The lower trace is the difference profile.

This result excludes the occurrence of static crystallographic distortions to structures with two inequivalent Co sites.

The growth in intensity of the low-angle reflections reveals that ferromagnetic order occurs at low temperature even in the sample with Sr content as small as 0.10. As shown in the inset of Fig. 6, this growth in intensity is most evident at the (1 1 0) position due to the very small nuclear structure factor for the corresponding crystallographic Bragg peak. No magnetic satellites have been detected, excluding the development of antiferromagnetic order of any kind, at least down to 2 K. The observation of ferromagnetic order for samples with $x<0.2$ is at variance with the results reported in Ref. 28, where a magnetic Bragg peak was observed only for $x\geq 0.2$.

At $T=4$ K, magnetic and nuclear Bragg peaks have the same linewidth, which is slightly larger than the instrument resolution. Although the linewidth of the magnetic (1 1 0) reflection becomes progressively broader with decreasing x, the correlation length for the magnetic order remains several hundreds of angstroms even for $x=0.10$. No temperature variation of the (1 1 0) peak shape could be detected for $x=0.20$, 0.25, and 0.30. On the contrary, for $x=0.15$ this peak becomes broader as the temperature is increased (Fig. 7); the ferromagnetic correlation length changes from about 700 Å below 80–90 K to about 300 Å for temperatures between 90 and 200 K. The magnetic intensity for the $x=0.10$ sample was too weak for an analysis of the temperature dependence of the line shape.

Rietveld analysis of the diffraction patterns was performed with the programs available in the GSAS (General

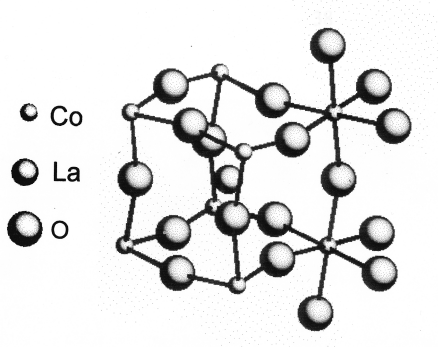

FIG. 9. The crystallographic structure of $La_{1-x}Sr_xCoO_3$ ($0\leq x\leq 0.30$). Only two CoO_6 polyhedra are shown for simplicity.

TABLE I. Cell parameters (a, α), oxygen fractional coordinate (x), isotropic temperature factors (B), and ordered magnetic moment (μ) for $La_{1-x}Sr_xCoO_3$ ($0.10 \leq x \leq 0.30$) at 2 K. The parameters are referred to the rhombohedral axes (space group $R\bar{3}c$, No. 167). The La(Sr) ions occupy the $2(a)$ sites with fractional coordinates $(\frac{1}{4},\frac{1}{4},\frac{1}{4})$, the Co is at $2(b)$, (0,0,0), and the O is at $6(e)$ $(x, \frac{1}{2}-x, \frac{1}{4})$.

Sr content	0.10	0.15	0.20	0.25	0.30
a (Å)	5.3647(1)	5.3713(1)	5.3807(2)	5.3864(1)	5.3933(3)
α (deg)	60.826(2)	60.758(2)	60.663(2)	60.605(2)	60.534(1)
Oxygen x	0.2010(2)	0.2032(2)	0.2051(3)	0.2081(2)	0.2102(2)
B_{La} (Å^2)	0.20(4)	0.18(3)	0.17(6)	0.16(4)	0.15(3)
B_{Co} (Å^2)	0.43(4)	0.42(3)	0.40(6)	0.39(4)	0.39(6)
B_O (Å^2)	0.65(4)	0.63(3)	0.62(6)	0.61(4)	0.60(2)
μ (μ_B)	0.3(1)	0.52(2)	1.26(5)	1.58(3)	1.71(2)

Structure Analysis System) suite of crystallographic routines.[36] Structure parameters, isotropic temperature factors, oxygen occupation factor, and cell parameters were determined from single or automatic sequential refinements. The scattering lengths used were $b_{La}=8.24$ fm, $b_{Sr}=7.02$ fm, $b_{Co}=2.49$ fm, and $b_O=5.805$ fm. The angular dependence of the magnetic scattering amplitude was described with the free-ion form factor $f(\sin\theta/\lambda)$ for Co^{3+} (the difference between the form factors for Co^{3+} and Co^{4+} being smaller than 2% in the investigated range of $\sin\theta/\lambda$).[37] The background was fitted with a 12th-order shifted Chebychev polynomial, and the shape of the Bragg peaks was described by a four-term pseudo-Voigt function. The final weighted pattern R index, R_{wp}, varied between 2% and 4%. Observed, calculated, and difference diffraction patterns for $La_{0.7}Sr_{0.3}CoO_3$ at 2 K are shown, as an example, in Fig. 8.

B. Variation of the structural parameters with Sr content at $T=2$ K

The crystal structure of $La_{1-x}Sr_xCoO_3$ ($0 \leq x \leq 0.30$) is shown in Fig. 9. The structural parameters at $T=2$ K, referred to the rhombohedral axes, are reported in Table I. The refinement of the oxygen occupancy confirmed that the investigated samples were oxygen stoichiometric within 0.8%. As shown in Fig. 10, the volume of the unit cell has an abrupt expansion as Sr^{2+} is introduced at small doping levels, but it increases linearly with the Sr content x for $x \geq 0.10$. The equilibrium Co-O bond length also makes a jump as the composition is changed from $x=0$ to 0.1, but it is scarcely influenced by a further increase of the Sr concentration up to $x=0.30$ (Fig. 11). The bond lengths for $x \geq 0.10$ are intermediate between those obtained from the sum of tabulated ionic radii,[38] namely 1.95 Å for HS Co^{3+} and 1.89 Å for LS Co^{3+}.

The rhombohedral distortion is due to the cooperative rotations of the $CoO_{6/2}$ polyhedra about the threefold axis of the ideal cubic perovskite structure, and it can be measured by the departure from 180° of the Co-O-Co angle, which also modulates the strength of the Co-O-Co interaction. On the other hand, the deviation from 90° of the O-Co-O angle gives a measure of the distortion of the cubic $CoO_{6/2}$ octahedra. As shown in Fig. 12, an increase of x results in a smaller and smaller rhombohedral distortion and in the straightening of the $CoO_{6/2}$ polyhedra, the corresponding angles varying almost linearly with x. The combined effect of these structural variations is to enhance the Co($3d$)-O($2p$)-Co($3d$) interactions, which broadens the σ^* band and is consistent with the occurrence of the semiconductor-to-metal transition with increasing x.

C. Temperature variation of the structural parameters

The temperature variation of the relevant bond angles for the $x=0.30$ sample is shown in Fig. 13. A similar behavior was observed for all the other investigated compositions. The structural modifications induced by an increase of temperature are very small up to about 50 K. At higher temperatures,

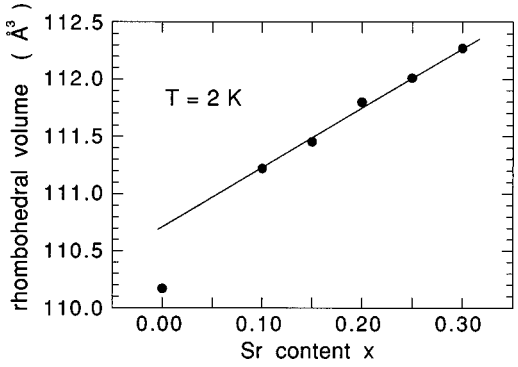

FIG. 10. Variation with x of the $La_{1-x}Sr_xCoO_3$ rhombohedral unit-cell volume. The linear fit for $0.10 \leq x \leq 0.30$ emphasizes the initial jump at small Sr^{2+} doping levels. Error bars are smaller than the size of the dots.

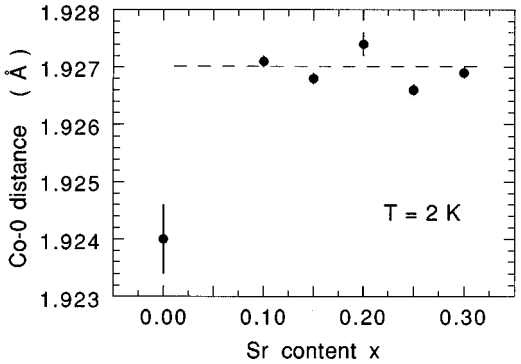

FIG. 11. Equilibrium Co-O bond length as a function of the Sr content x, at $T=2$ K. After an initial jump, the Co-O distance remains almost constant as x is increased up to 0.30.

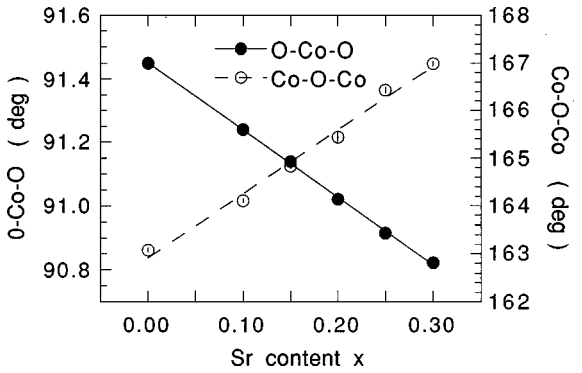

FIG. 12. Variation with the Sr content x of the Co-O-Co and O-Co-O angles, at $T=2$ K. Error bars are smaller than the size of the symbols.

the distortion decreases with increasing temperature in the same way it does at 2 K with increasing Sr concentration: the O-Co-O angle moves towards 90°, the value corresponding to perfect $CoO_{6/2}$ octahedra, and the rhombohedral distortion decreases as the Co-O-Co angle becomes larger. The variation seems to saturate on warming above the Curie point.

As shown in Fig. 14, a small but significant increase of the equilibrium Co-O distance was observed on warming for all the samples. It is interesting to notice that the Co-O bond length is largest for $x=0.20$, close to the semiconductor-to-metal transition. A peculiar behavior of the Co-O distance is observed at $x=0.30$ (Fig. 15). At this composition, the Co-O bond length remains almost constant up to about 230 K, near the Curie point T_C, and increases dramatically in the paramagnetic phase. As discussed below, this behavior can be attributed to a transition from itinerant to polaronic conduction at T_C; magnetic polarons are stabilized above T_C.

The temperature variation of the rhombic cell parameter a_R is plotted in Fig. 16 for $x=0.10$, 0.15, 0.20, and 0.25. The lattice thermal expansion is typical for a solid and can be fitted to the formula

$$a_R(T)=a_0\left\{1+\frac{\alpha_L T_E}{2}\left[\coth\left(\frac{T_E}{2T}\right)-1\right]\right\},$$

which is obtained from the Grüneisen approximation for the anharmonic phonon effects and the Einstein model for the constant-volume specific heat; a_0 is the value of a_R at $T=0$, T_E is the Einstein temperature, and α_L is the linear

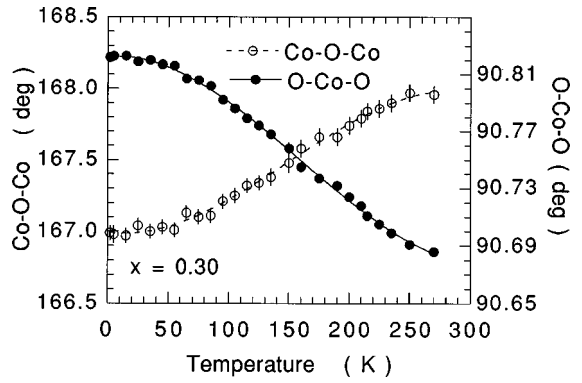

FIG. 13. Temperature variation of the Co-O-Co and O-Co-O angles for $La_{0.7}Sr_{0.3}CoO_3$.

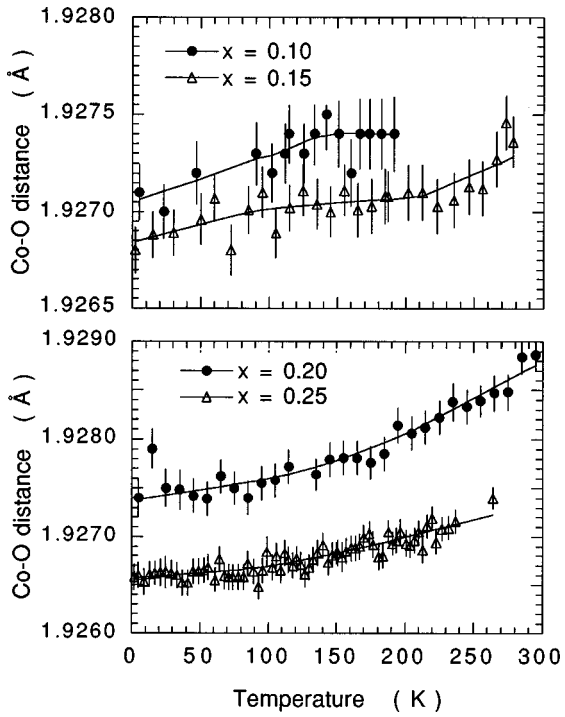

FIG. 14. Temperature variation of the equilibrium Co-O distance for samples with $0.10\leqslant x\leqslant 0.25$. The expansion between 2 K and room temperature is smaller than 0.07% for all the samples. The largest Co-O distance is attained at $x=0.20$, close to the semiconducting-to-metal transition boundary.

thermal expansion coefficient for $T\gg T_E$. The solid lines in Fig. 16 are calculations with the above formula for the T_E and α_L values shown in Fig. 17 and the a_0 values given in Table I. To be noted are the reductions of both T_E and α_L that accompany the transition from the semiconducting phase, at $x=0$, to the metallic phase, at $x=0.20$.

For $x=0.30$, a regular thermal expansion is observed as long as the sample remains in the ferromagnetic phase. As shown in Fig. 18, a departure from the Grüneisen behavior is evident above T_C; the lattice parameter increases more rapidly than expected. The observed deviations from the calculated values are correlated to the anomalous temperature variation of the Co-O distance $d_{\text{Co-O}}$, as can be seen in the inset of Fig. 18, where the ratio $[d_{\text{Co-O}}(T)-d_{\text{Co-O}}(0)]/d_{\text{Co-O}}(0)$ is compared to the relative difference $(a_{R,\text{obs}}-a_{R,\text{calc}})/a_{R,\text{calc}}$.

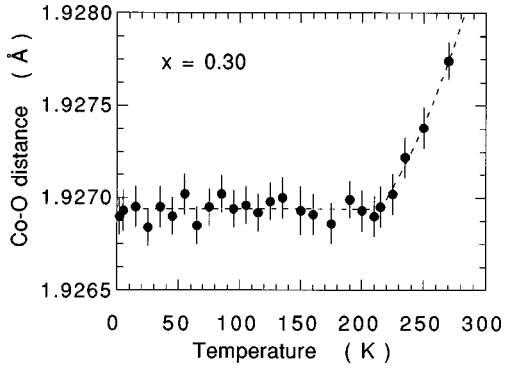

FIG. 15. The equilibrium Co-O bond length as a function of temperature for $La_{0.7}Sr_{0.3}CoO_3$. A dramatic increase occurs above 230 K. The broken line is a guide to the eye.

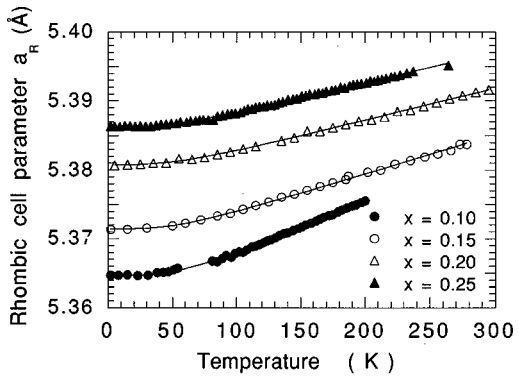

FIG. 16. Temperature dependence of the rhombohedral lattice parameter a_R for $La_{1-x}Sr_xCoO_3$ ($0.10 \leqslant x \leqslant 0.25$). The solid line is a fit to the Grüneisen-Einstein model with the parameters plotted in Fig. 17.

D. Magnetic order parameter

The Rietveld analysis of the magnetic-intensity distribution indicates a ferromagnetically ordered low-temperature phase with the Co magnetic moments oriented along the (1 0 0) direction of the rhombohedral cell. The values of the ordered moment at $T=2$ K are given in Table I; they vary with x in a nonlinear way, from $\mu=0.3(1)\mu_B$ for $x=0.10$ to $\mu=1.71(2)\mu_B$ for $x=0.30$.

For the $x=0.10$ sample, the magnetic contribution to the diffraction profile was too weak to allow a proper determination of the ordered moment through the Rietveld method, and we limited our analysis to the evaluation of the magnetic moment at 2 K from the integrated intensity of the (1 1 0) peak. For the other compositions, the temperature dependence of the magnetic moment was refined, and the results are compared in Fig. 19 with the Brillouin function for $J=2$. Approaching the Curie point, the magnetic moment scales as t^{β}, where $t=1-T/T_C$, with almost the same Curie temperature $T_C=227\pm4$ K for all the samples and β close to 0.4. It should be noted that a considerably smaller value of β was obtained in the La manganates due to an important single-ion anisotropy term in the Hamiltonian for that system.[39] A deviation from the mean-field prediction is evident for both the $x=0.15$ and the $x=0.20$ samples, with a step near $0.5T_C$ in the temperature region where the magnetic Bragg peak becomes sharper and the slope of the susceptibility curve changes. A much smaller step is also visible

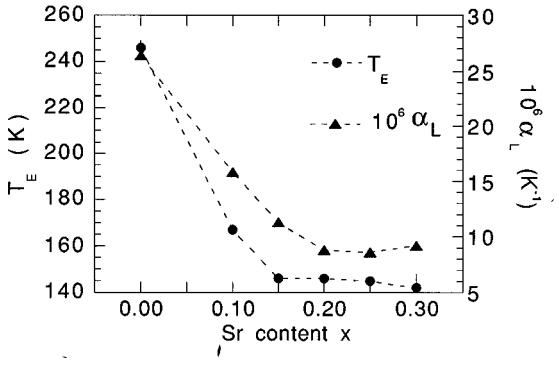

FIG. 17. Variation of the Einstein temperature T_E and the linear thermal expansion coefficient for $T \gg T_E$, α_L, with the Sr content x.

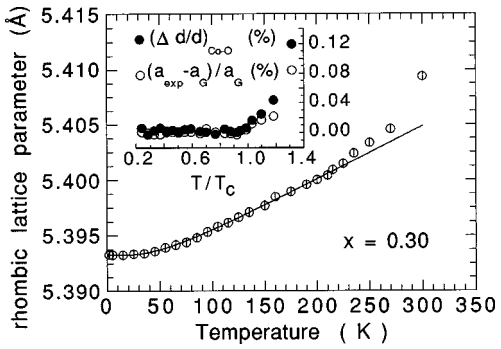

FIG. 18. Temperature dependence of the rhombohedral lattice parameter a_R for $La_{0.7}Sr_{0.3}CoO_3$. The solid line is a fit to the Grüneisen-Einstein model. The inset shows the comparison between the relative variation $[d_{Co\text{-}O}(T)-d_{Co\text{-}O}(0)]/d_{Co\text{-}O}(0)$ of the Co-O distance and the relative departure of the lattice parameter from the value predicted by the Grüneisen-Einstein formula, $(a_{R,obs}-a_{R,calc})/a_{R,calc}$.

in the $\mu(T)$ curve for the $x=0.30$ sample, while a strong fluctuation tail seems to be present above the scaling value of T_C for $x=0.25$.

VI. DISCUSSION

In $LaCoO_3$, the transition of the cobalt LS configurations to a higher-spin configuration with increasing temperature introduces antibonding e electrons, which increases the equilibrium Co-O bond length. A continuous increase in the fraction of higher-spin Co^{3+} ions gives a smooth transition that translates to an unusually large thermal expansion of the lattice. For localized electrons, a LS state normally transforms to a HS state; but it was recognized that stabilization of an IS state might be expected in a solid where e electrons are transformed into itinerant-electron σ^*-band states, and a subsequent LDA+U calculation[40] has suggested that above a critical Co-O bond length the IS state would be more stable. Photoemission and x-ray spectroscopy studies support a smooth transition to a higher spin state.[41] However, dynamic Jahn-Teller deformations observed[25] at isolated IS cobalt in $LaCoO_3$ indicate neighboring LS trivalent cobalt confines the

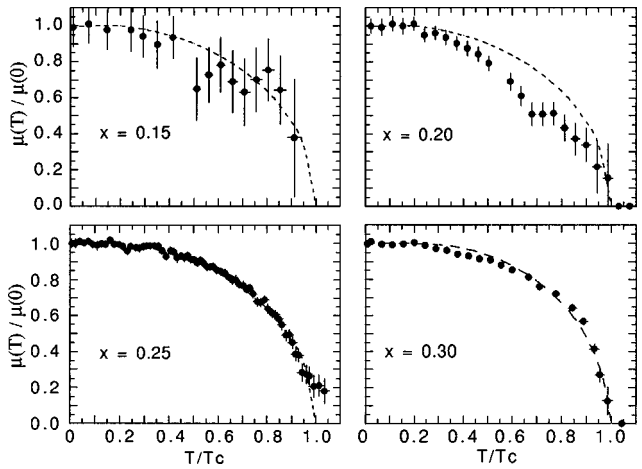

FIG. 19. Reduced magnetic ordered moment $\mu/\mu(T=0)$ vs reduced temperature T/T_C. The broken line is the mean-field prediction for the $J=2$ Brillouin function.

e electrons to localized t^5e^1 IS configurations below 350 K. With increasing concentrations of higher-spin configurations, whether HS or IS, the formation of IS metallic clusters has been predicted[16,17] for the interval $350<T<650$ K, a global IS state being stabilized only above 650 K. The anomalous thermal expansion observed[42] near 500 K may reflect consolidation of the IS clusters rather than addition of some HS configurations.

High-resolution electron microscopy provides evidence for an inhomogeneous distribution of the Sr^{2+} ions in the $La_{1-x}Sr_xCoO_3$ system. The Co(IV):t^5e^0 ions are in a low-spin state, the stronger Co(IV)-O covalent bonding stabilizes IS Co^{3+}:t^5e^1 at the neighboring cobalt atoms to lowest temperatures, and the e^1 electrons are shared with the Co(IV) ions within an IS molecular-orbital cluster. The shared e^1 electrons couple the localized t^5 configurations ferromagnetically, so the clusters become superparamagnetic within a Co^{3+}-ion matrix in which the IS configurations remain localized and paramagnetic below room temperature. Loss of oxygen above room temperature has restricted the temperature range of measurement of Sr-substituted samples. The observation of Sr^{2+} ion clustering indicates an instability relative to the formation of Sr^{2+}-rich clusters containing hole-rich IS configurations within a hole-poor matrix. The degree of such chemical heterogeneity would depend on the thermal history of the sample and its eventual oxidation state, so the critical concentration for the onset of long-range ferromagnetic order may differ from one sample to another, from one laboratory to another. On the other hand, there was little evolution of the degree of chemical heterogeneity in our samples on going from $x=0.15$ to 0.30 whereas there is a strong evolution of the size of the ferromagnetic IS clusters. Therefore, we presume that mobile two-phase interfaces are also present as a result of dynamic cooperative oxygen displacements that segregate, below room temperature, ferromagnetic hole-rich regions of IS states with itinerant σ^* electrons from hole-poor regions in which the higher-spin configurations at Co^{3+} ions remain localized and paramagnetic due to their isolation by neighboring LS Co(IV) ions. We employ this assumption to interpret the unusual evolution with x of the physical properties in the $La_{1-x}Sr_xCoO_3$ system.

The composition-driven transition to the metallic, ferromagnetic phase at $x=0.2$ can be considered to occur at a percolation threshold for IS metallic clusters; the threshold composition would vary with the size of the IS clusters and hence with the strength of an applied magnetic field above the long-range ferromagnetic-ordering temperature T_C; below T_C, the Weiss molecular field stabilizes larger IS metallic clusters. The ferromagnetic superexchange coupling between hole-rich ferromagnetic clusters below T_C is via alternating LS and localized IS Co^{3+}-ion states of the hole-poor matrix; but a decrease in the concentration of localized IS states at lower temperatures can break this superexchange coupling, thereby reducing the Weiss molecular field that induces growth of the ferromagnetic clusters beyond percolation. In the compositional range $0.15<x<0.3$, the variability of the critical composition for percolation with the Weiss molecular field of the hole-poor matrix is manifest by the appearance below T_C of a metallic state (beyond percolation) on cooling through T_C, but with a reentrant insulating phase (below percolation) at lowest temperatures.[16] The large magnetoresistance near T_C in this compositional range[8] reflects the growth to percolation of the metallic, ferromagnetic clusters in an applied magnetic field.

The step in the magnetization versus temperature curves of the $x=0.15$ and 0.20 samples, Fig. 19, may be attributed to an increase in the global T_C with increasing percolation above 150 K; the local T_C for the superparamagnetic clusters does not change significantly with x. An increase in the size of the metallic clusters at percolation would also give an increase in the mean cobalt spin. By $x=0.30$, percolation is established, and the deviation of the magnetization from mean-field behavior is small.

A spin-only magnetization for IS $La_{1-x}Sr_xCoO_3$ would be $(2-x)\mu_B$/Co; the LDA+U calculation[40] gave $2.1\mu_B$/Co for $x=0$. The observed magnetizations for ferromagnetic $La_{1-x}Sr_xCoO_3$ compositions are consistent with a ferromagnetic IS matrix containing LS Co(IV)-poor clusters that decrease in volume with increasing $x\geqslant 0.25$. However, even in the $x=0.10$ sample the widths of the magnetic Bragg peaks in the neutron-diffraction profiles indicate a spin-correlation length of several hundred angstroms. This observation indicates ferromagnetic coupling between clusters is occurring via superexchange interactions before the percolation threshold is reached.

The anomalous thermal expansion of the $x=0.30$ sample, Fig. 18, deserves special attention. A small-angle-neutron-scattering (SANS) experiment performed on the same specimen used in the present investigation has shown a magnetic signal that increases with temperature to a sharp maximum a little above T_C,[43] suggesting a growth to a maximum at T_C in the number of ferromagnetic regions with sizes of the order of 10–15 Å on warming through T_C. Similar observations for Ca-doped $LaMnO_3$ have been interpreted to indicate a break-up of long-range ferromagnetic order above T_C into magnetic polarons stabilizing regions of short-range ferromagnetic order.[5] However, a maximum in the thermoelectric power suggests the regions of short-range ferromagnetic order trap out mobile polarons from the matrix, which indicates the ''magnetic polarons'' represent a second electronic phase.[7] This interpretation can also be applied to $La_{0.7}Sr_{0.3}CoO_3$, which shows an increase in spin-disorder scattering on the approach to T_C and a maximum in the thermoelectric power a little above T_C (Ref. 16) but with retention of a metallic temperature dependence of the conductivity in the paramagnetic matrix to room temperature.

In a SANS experiment, the energy of the scattered neutron beam is not analyzed and, therefore, what is obtained is the magnetic response integrated over a large energy window centered at zero energy transfer. This means that the observed clustering effect, which is also manifest in the strong deviation of the magnetic susceptibility from Curie-Weiss behavior, may be dynamic in origin as would occur for short-range ferromagnetic fluctuations.

A transition from an itinerant electron to a cluster or polaronic state can account for the dramatic increase in the Co-O bond length on heating through T_C. According to the virial theorem of classical mechanics, which states for central-force fields that $2\langle K\rangle+\langle V\rangle=0$, an increase in the mean kinetic energy $\langle K\rangle$ of the electrons on changing from itinerant to polaronic behavior must be compensated by an

increase in the magnitude of their negative mean potential energy $|\langle V\rangle|$. For antibonding electrons, an increase in the Co-O bond length stabilizes the Co(IV)/Co(III) couple, thereby increasing $|\langle V\rangle|$. In order to maintain itinerant-electron behavior on the approach to a transition to polaronic behavior, a perovskite system may maintain a fixed M-O distance while straightening the M-O-M bond angle, as is observed in the $x=0.30$ sample; the rhombohedral distortion of the perovskite structure is seen to diminish on heating, the $CoO_{6/2}$ polyhedra moving towards perfect octahedra.

VII. CONCLUSIONS

High-resolution electron microscopy, linear, and nonlinear magnetic susceptibility and neutron-diffraction experiments have been performed to study the crystallographic structure and the magnetic order in the rhombohedrally distorted perovskites $La_{1-x}Sr_xCoO_3$ ($x=0.10$, 0.15, 0.20, 0.25, and 0.30). The parent compound $LaCoO_3$ has all low-spin Co(III):t^6e^0 configurations at lowest temperatures, but thermal excitation of higher-spin configurations introduces an anomalously large thermal expansion. The higher-spin configurations appear to be IS t^5e^1 and to remain isolated and localized below 350 K; above 650 K, all the trivalent cobalt is transformed to IS states with itinerant e electrons occupying a narrow σ^* band.

Doping with Sr introduces LS Co(IV):t^5e^0 ions that stabilize IS Co^{3+} near neighbors having their e electrons delocalized over molecular orbitals of a hole-rich cluster. Retention of IS configurations to lowest temperatures produces a sharp increase in the unit-cell volume and mean Co-O bond length at 2 K in the range $0<x<0.10$, Figs. 10 and 11. The delocalized e electrons provide strong ferromagnetic coupling of the localized t^5 configurations at the cobalt atoms of a hole-rich cluster. Below room temperature, the higher-spin configurations of the hole-poor matrix remain localized, and at low Sr doping ($x<0.05$) the hole-rich clusters become superparamagnetic. With increasing x, the superparamagnetic clusters become coupled ferromagnetically to one another via superexchange through the hole-poor matrix, and by $x=0.10$ long-range ferromagnetic order of a small volume fraction of the sample was found. This volume may depend, for a given x, on the preparation conditions. The volume of the superparamagnetic clusters grows in a magnetic field, and in the range $0.15\leqslant x\leqslant 0.25$ the volume of the hole-rich clusters approaches percolation. In this compositional range, percolation may be induced above T_C by the application of a magnetic field to give a large negative magnetoresistance; on cooling below T_C, the Weiss internal magnetic field induces percolation, but on further cooling a reentrant break-up of percolation occurs as the ferromagnetic coupling between hole-rich clusters is weakened by a decrease in the concentration of higher-spin cobalt in the matrix. At $x=0.30$, percolation is retained at all temperatures below T_C with retention of a constant Co-O bond length; but SANS shows an increase in the concentration of short-range ferromagnetic clusters that reaches a maximum at T_C; above T_C, the mean Co-O bond length increases sharply with temperature indicative of a confinement of the delocalized electrons to clusters of finite volume above T_C even though a metallic temperature dependence of the conductivity is retained to room temperature. The paramagnetic susceptibility, Fig. 5, confirmed retention of extensive short-range ferromagnetic order for 60 K above T_C.

Electron microscopy showed evidence of Sr-rich phases in the $x=0.15$ and 0.30 samples indicating that segregation of a hole-rich phase persists above room temperature and attracts Sr^{2+} ions. However, the absence of an evolution of the chemical heterogeneity between $x=0.15$ and 0.30 would seem to indicate that not all of the hole-rich clusters are pinned at the Sr-rich planes and that certainly the growth of the ferromagnetic hole-rich clusters in a magnetic field is not inhibited by any pinning that may occur.

Note added in proof. This procedure involves annealing at 1000 °C. Anilkumar *et al.* [J. Appl. Phys. **83**, 7375 (1998)] have shown that, for $x=0.15$, phase segregation may occur under our experimental conditions. However, an anneal at $T\geqslant 1200$ °C gave them a homogeneous product with a spin-glass transition temperature $T_g=75$ K.

ACKNOWLEDGMENTS

This work was partially supported by the MURST of Italy, and the DGICYT of Spain, under Contract No. MAT98-0416. J.B.G. thanks the NSF for support. We are grateful to Dr. Pierre Convert and Dr. Thomas Hansen of the Institute Laue Langevin in Grenoble, France, for their help during the neutron-diffraction experiment.

[1] S. Jin, T. H. Tiefel, M. McCormack, R. A. Fastnacht, R. Ramesh, and L. H. Chen, Science **264**, 413 (1994).

[2] H. Röder, J. Zang, and A. R. Bishop, Phys. Rev. Lett. **76**, 1356 (1996).

[3] G. Zhao, K. Conder, H. Keller, and K. A. Müller, Nature (London) **381**, 676 (1996).

[4] M. Jaime, H. T. Hardner, M. B. Salamon, M. Rubinstein, P. Dorsei, and D. Emin, Phys. Rev. Lett. **78**, 951 (1997).

[5] J. M. De Teresa, M. R. Ibarra, P. A. Algarabel, C. Ritter, C. Marquina, J. Blasco, J. Garcia, A. del Moral, and Z. Arnold, Nature (London) **386**, 256 (1997).

[6] W. Archibald, J-S. Zhou, and J. B. Goodenough, Phys. Rev. B **53**, 14 445 (1996).

[7] J. B. Goodenough and J-S. Zhou, in *Materials for Electrochemical Energy Storage and Conversion II*, edited by D. S. Gingley, D. M. Doughty, B. Scrosati, T. Takamura, and Z. Zhang, MRS Symposia Proceedings No. 47Y (Materials Research Society, Pittsburgh, 1998).

[8] G. Briceño, H. Chang, X. Sun, P. G. Schultz, and X.-D. Xiang, Science **270**, 273 (1995).

[9] T. Saitoh, T. Mizokawa, A. Fujimori, M. Abbate, Y. Takeda, and M. Takano, Phys. Rev. B **56**, 1290 (1997).

[10] F. Munakata, H. Takahashi, Y. Akimune, Y. Shichi, M. Tanimura, Y. Inoue, R. Itti, and Y. Koyama, Phys. Rev. B **56**, 979 (1997).

[11] N. Gayathri, A. K. Raychaudhuri, S. K. Tiwary, R. Gundakaram,

A. Arulraj, and C. N. R. Rao, Phys. Rev. B **56**, 1345 (1997).
[12] M. R. Ibarra, R. Mahendiran, C. Marquina, B. Garcia-Landa, and J. Blasco, Phys. Rev. B **57**, R3217 (1998).
[13] S. Yamaguchi, H. Taniguchi, H. Takagi, T. Arima, and Y. Tokura, J. Phys. Soc. Jpn. **64**, 1885 (1995).
[14] R. Mahendiran and A. K. Raychaudhuri, Phys. Rev. B **54**, 16 044 (1996).
[15] V. Golovanov, L. Mihaly, and A. R. Moodenbaugh, Phys. Rev. B **53**, 8207 (1996).
[16] M. A. Señarís-Rodríguez and J. B. Goodenough, J. Solid State Chem. **118**, 323 (1995).
[17] M. A. Señarís-Rodríguez, and J. B. Goodenough, J. Solid State Chem. **116**, 224 (1995).
[18] P. M. Raccah and J. B. Goodenough, Phys. Rev. **155**, 932 (1967).
[19] J. B. Goodenough, Mater. Res. Bull. **6**, 967 (1971).
[20] G. Thornton, B. C. Tofield, and A. W. Hewat, J. Solid State Chem. **61**, 301 (1986).
[21] N. Menyak, K. Dwight, and P. M. Raccah, J. Phys. Chem. Solids **28**, 599 (1967).
[22] K. Asai, O. Yokokura, N. Nishimori, H. Chou, J. M. Tranquada, G. Shirane, S. Higuchi, Y. Okajima, and K. Kohn, Phys. Rev. B **50**, 3025 (1994).
[23] J. B. Goodenough, J. Phys. Chem. Solids **6**, 287 (1958).
[24] V. G. Bhide, D. S. Rajoria, G. R. Rao, and C. N. R. Rao, Phys. Rev. B **6**, 1021 (1972).
[25] S. Yamaguchi, Y. Okimoto, and Y. Tokura, Phys. Rev. B **55**, R8666 (1997).
[26] E. Iguchi, K. Ueda, and W. H. Jung, Phys. Rev. B **54**, 17 431 (1996).
[27] J. Mira, J. Rivas, R. D. Sanchez, M. A. Señaris-Rodriguez, D. Fiorani, D. Rinaldi, and R. Caciuffo, J. Appl. Phys. **81**, 5753 (1997).
[28] V. G. Sathe, A. V. Pimpale, V. Siruguri, and S. K. Paranjpe, J. Phys.: Condens. Matter **8**, 3889 (1996).
[29] R. Mahendiran, A. K. Raychaudhuri, A. Chainani, and D. D. Sarma, J. Phys.: Condens. Matter **7**, L561 (1995).
[30] P. A. Stadelmann, Ultramicroscopy **21**, 131 (1987).
[31] M. Itoh, I. Natori, S. Kubota, and K. Motoya, J. Phys. Soc. Jpn. **63**, 1486 (1994).
[32] M. Itoh and I. Natori, J. Phys. Soc. Jpn. **64**, 970 (1995).
[33] K. Binder and A. P. Young, Rev. Mod. Phys. **58**, 801 (1986).
[34] S. Mukherjee, R. Ranganathan, P. S. Anilkumar, and P. A. Joy, Phys. Rev. B **54**, 9267 (1996).
[35] S. B. Oseroff, M. Torikachvili, J. Singley, S. Ali, S.-W. Cheong, and S. Schultz, Phys. Rev. B **53**, 6521 (1996).
[36] A. C. Larson and R. B. von Dreele, Los Alamos National Laboratory Report No. LA-UR-86-748 (1987).
[37] P. J. Brown, in *International Tables for Crystallography*, edited by A. J. C. Wilson (Kluwer, Dordrecht, 1995), Vol. C, p. 391.
[38] R. D. Shannon, Acta Crystallogr., Sect. A: Cryst. Phys., Diffr., Theor. Gen. Crystallogr. **32**, 751 (1976).
[39] F. Moussa, M. Hennion, J. Rodriguez-Carvajal, H. Moudden, L. Pinsard, and A. Revcolevschi, Phys. Rev. B **54**, 15 149 (1996).
[40] M. A. Korotin, S. Yu. Ezhov, I. V. Solovyev, V. I. Anisimov, D. I. Khomskii, and G. A. Sawatzky, Phys. Rev. B **54**, 5309 (1996).
[41] T. Saitoh, T. Mizokawa, A. Fujimori, M. Abbate, Y. Takeda, and M. Takano, Phys. Rev. B **55**, 4257 (1997).
[42] K. Asai, A. Yoneda, O. Yokokura, J. M. Tranquada, G. Shirane, and K. Kohn, J. Phys. Soc. Jpn. **67**, 290 (1998).
[43] R. Caciuffo, J. Mira, J. Rivas, M. A. Señarís-Rodríguez, P. G. Radaelli, F. Carsughi, D. Fiorani, and J. B. Goodenough, Europhys. Lett. (to be published).